CHEMISTRY JOURNAL OF MOLDOVA. General, Industrial and Ecological Chemistry. 2026, 21(1), 112-124
ISSN (p) 1857-1727 ISSN (e) 2345-1688
http://cjm.ichem.md
https://doi.org/10.19261/cjm.2026.1476

SYNTHESIS AND CHARACTERIZATION OF A CONJUGATED MULTIFUNCTIONAL OLIGOMER DERIVED FROM PARA-PHENYLENEDIAMINE AND CATECHOL

Ramil Rzayev [a,b,c*], Natalia Sucman [a], Eduard Monaico [d], Ion Geru [a], Alina Nicolescu [e,f], Calin Deleanu [e,f], Valentin Batır [g], Bakhtiyar Mammadov [c], Rena Akhmedova [c], Fliur Macaev [a]

[a] *Institute of Chemistry, Moldova State University, 3, Academiei str., Chisinau MD-2028, Republic of Moldova*
[b] *Department of Chemical Engineering, Baku Engineering University, 120, Hasan Aliyev str., Baku, Absheron, AZ0101, Azerbaijan*
[c] *Institute of Polymer Materials, Azerbaijan National Academy of Sciences, 124, Vurgun str., Sumgait, AZ5004, Azerbaijan*
[d] *National Center for Materials Study and Testing, Technical University of Moldova, 168, Stefan cel Mare bvd., Chisinau MD-2004, Republic of Moldova*
[e] *"Petru Poni" Institute of Macromolecular Chemistry, 41 A, Aleea Grigore Ghica Voda, RO-700487, Iasi, Romania.*
[f] *"Costin D. Nenitescu" Institute of Organic and Supramolecular Chemistry, 202 B, Independentei spl., RO-060023 Bucharest, Romania*
[g] *Institute of Applied Physics, Moldova State University, 5, Academiei str., Chisinau MD-2028, Republic of Moldova*
[*] *e-mail: ramilrzayev81@gmail.com*

Abstract. A *p*-phenylenediamine–catechol-based oligomer was synthesized *via* oxidative polycondensation in an acidic medium under ultrasonic irradiation, employing potassium persulfate as the oxidant to obtain an oligomeric material. The resulting material was characterized by Fourier-transform infrared (FT-IR) spectroscopy, ultraviolet–visible (UV-Vis) spectroscopy, thermogravimetric analysis (TGA), nuclear magnetic resonance (NMR) spectroscopy, scanning electron microscopy (SEM), X-ray diffraction, and electron spin resonance (ESR) spectroscopy. FT-IR and NMR analyses confirm that the reaction conditions (with and without surfactant, in presence of ethanol) significantly affect the composition of the resulting materials. It was established that, depending on the reaction conditions, the formation of a trimer composed of two *para*-phenylenediamine units and one catechol moiety, as well as the formation of poly-1,2-dihydroxybenzene, occurs in different ratios. No products of the individual polycondensation of *p*-phenylenediamine were detected. UV-Vis spectroscopy indicates wide-band-gap semiconducting behavior, with an optical band gap of approximately 4.7 eV estimated from the Tauc plot analysis. TGA shows the oligomer is stable up to ~270°C. SEM revealed an irregular, predominantly flake-like fragmented surface morphology without well-defined individual particles. ESR confirmed unpaired electrons within the oligomer structure. Temperature-dependent conductivity measurements revealed an unusual conductivity trend, where conductivity slightly increased with decreasing temperature within the investigated range. At room temperature, the measured conductivity is 1.06×10^{-7} S/cm.

Keywords: polycatechol, 1,4-diaminobenzol, 1,2-benzenediol, potassium persulfate, oxidative polymerization.

Received: 2 May 2026/ Revised final: 5 June 2026/ Accepted: 8 June 2026

Introduction

Aromatic amines are an important group of compounds with many industrial and technological applications due to their unique chemical and physical properties [1-3]. Among them, polyaniline (PANI), one of the earliest known conducting polymers, was first synthesized in the 19th century, *via* the polymerization of aniline in an acidic medium [4-6]. PANI has drawn extensive attention due to its unique property profile, including electrical conductivity [7,8], environmental stability, favourable magnetic and optical properties [9,10], redox activity, low density, and ease of synthesis [11]. These features have enabled its integration into various devices such as LEDs [12], OLEDs [13], solar cells [14], sensors, capacitors [15], electrochemical systems [16], batteries [17], and anti-static coatings [18], as well as its application in electromagnetic shielding [19], and other advanced electronic and optical technologies. Nonetheless, the widespread use of this material is hindered by its limited

solubility in organic solvents and poor processability.

Phenylenediamines, key derivatives of aniline, possess two primary amino groups that facilitate the oxidative coupling reactions of monomers [20-24]. Among these, *para*-phenylenediamine (PPD) is one of the most extensively studied diaminobenzenes, undergoing oxidative polymerization to yield poly-(*p*-phenylenediamine) a conjugated polymer distinguished by its remarkable redox activity, excellent chemical stability, and broad application potential in fields such as electrochemistry, dyes, and the rubber industry [25-30].

Phenol and its derivatives are a versatile class of compounds that have attracted significant attention due to their exceptional properties, such as excellent antioxidant activity, chemical reactivity, thermal and chemical stability, and wide applicability in pharmaceuticals, cosmetics, polymers, and their potential for use in conducting polymers and electrochemical devices [31-35].

Catechol (1,2-benzenediol), a key phenolic derivative, is distinguished by its two adjacent hydroxyl groups, which impart strong antioxidant capacity, metal-chelating ability, and enhanced chemical reactivity [36].

Catechol-based systems represent an important and versatile platform with applications in adhesives and coatings, smart polymers, biomedical materials, antimicrobial polymers, and related fields [37-40].

Although numerous research articles address the synthesis, characterization, and applications of poly-*para*-phenylenediamine [41,42] and poly-phenols, the copolymerization of 1,2-dihydroxybenzene with PPD remains underexplored, with only a limited number of studies [43,44].

Given the growing interest in polymers with diverse functional groups [45], copolymerizing PPD with catechol offers an effective strategy to integrate the beneficial properties of both monomers, yielding hybrid materials with improved electrical conductivity, greater mechanical flexibility, and superior thermal stability, thereby broadening their potential for a range of applications.

The aim of this study was to investigate the polycondensation of *para*-phenylenediamine in the presence of 1,2-dihydroxybenzene, to determine the structure of the resulting products, and to evaluate the influence of reaction conditions on the course of oxidative polycondensation, with a particular focus on the formation of materials exhibiting electrical conductivity and on identifying the most favourable conditions for obtaining products with desirable functional properties.

In particular, the study focused on identifying the products formed under different conditions: in an aqueous acidic medium with and without surfactant, as well as in an aqueous acidic medium with the addition of organic solvents, both in the presence and absence of surfactant. In addition, the physicochemical characteristics of the obtained materials were studied using a range of analytical methods included spectroscopic methods such as nuclear magnetic resonance (NMR), Fourier-transform infrared (FT-IR), and ultraviolet–visible (UV-Vis) spectroscopy, microscopic and structural analysis used scanning electron microscopy (SEM) and x-ray diffraction (XRD), thermal and electronic properties were assessed by thermogravimetric analysis (TGA) and electron spin resonance (ESR), conductivity was measured with the four-probe method.

Experimental

Materials

Para-phenylenediamine (≥ 98%) (PPD) and 1,2-benzenediol (1,2-BD) (catechol, ≥ 99%) were used as monomers without further purification. Potassium persulfate (PPS, $K_2S_2O_8$, ≥ 99%) served as the oxidizing agent. Dodecyl amine (≥ 99%) used as surfactant. Hydrochloric acid (HCl, 37 vol%) was diluted to prepare a 1.0 M aqueous solution for the acidic medium. Ethanol (96%) and distilled water were used for washing the final product. All chemicals and solvents were purchased from Sigma–Aldrich (Germany). Deionized water was used throughout all the experimental processes.

Methods and instruments

Synthesis of PPD / 1,2-benzenediol copolymer under ultrasonic irradiation

Method A. The oxidative polycondensation of PPD with 1,2-benzenediol was conducted in 1.0 M HCl using potassium persulfate ($K_2S_2O_8$) as the oxidant. PPD (25 mmol, 2.7 g) and 1,2-benzenediol (25 mmol, 2.75 g) were dissolved in 50 mL of 1.0 M HCl in a 250 mL three-neck round-bottom flask equipped with an ultrasonic probe, a thermometer, and a water-cooled condenser. The reaction mixture was maintained at 0–15°C under continuous stirring. Prior to oxidation, the solution was sonicated for 20 min to ensure complete homogenization of the monomers, after which the polymerization was initiated. Upon completion of the reaction, the mixture was allowed to cool to room temperature, then isolated by vacuum filtration and washed

thoroughly with 500 mL of deionized water to remove any unreacted monomers, inorganic residues, and excess acid. Further purification was performed by repeatedly washing the filtrate with ethanol until it became clear. The product was dried in a vacuum oven at 60°C for 48 h to obtain a dark green powder. The synthesized compound is a black solid substance soluble in polar organic solvents (DMSO, DMF, acetone, etc).

Method B. First, PPD (25 mmol, 2.7 g) and 1,2-benzenediol (25 mmol, 2.75 g) were dissolved in a mixture of 50 mL 1.0 M HCl and 50 mL ethanol inside a 250 mL three-neck flask (equipped with ultrasonic probe, thermometer, and condenser) at 0–15°C. Once complete dissolution was achieved, 0.54 g dodecyl amine (DDA) was added to the solution. The mixture was then sonicated for 20 min. After sonication, potassium persulfate ($K_2S_2O_8$, 25 mmol, 6.275 g dissolved in 50 mL water) was added dropwise over 30 min during ongoing sonication. Following this addition, the reaction was maintained for 6 h. Throughout the reaction, the mixture gradually changed from light brown to dark green, indicating oxidative polymerization. Importantly, the entire polycondensation was carried out in 1.0 M HCl, using $K_2S_2O_8$ as the oxidant.

Method C. First, PPD (25 mmol, 2.7 g) and 1,2-benzenediol (25 mmol, 2.75 g) were dissolved in 50 mL of 1.0 M HCl in a 250 mL three-neck round-bottom flask equipped with an ultrasonic probe, thermometer, and water-cooled condenser. Dodecylamine (DDA) was then added as a surfactant, and the mixture was sonicated for 20 min to ensure complete monomer homogenization. After homogenization, the reaction mixture was kept at 0–15°C under continuous stirring. Polymerization was initiated by adding potassium persulfate ($K_2S_2O_8$) as the oxidant.

4,5-bis(4-aminophenylamino)cyclohexa-3,5-diene-1,2-dione ***1***. FT-IR (ν, cm^{-1}) 3218, 3016, 2867, 2591, 2287, 1706, 1604, 1564, 1506, 1408, 1420, 134, 1285, 1223, 1168, 1130, 1103, 1060, 1017, 968, 898, 819, 711. UV- 200–260 nm, 280–350 nm, 450 nm. TGA- 150°C, 260-300°C. ^{1}H NMR (400 MHz, DMSO-d_6) δ 9.24 (s, 2H, NH), 7.32–7.18 (m, 4H), 7.08–6.95 (m, 4H), 5.68 (s, 2H). ^{13}C NMR (101 MHz, DMSO-d_6) δ 179.1, 148.7, 145.1, 125.3, 119.2, 115.7, 94.3.

Poly-(1.2-dihydroxybenzene) ***2***. FT-IR (*ν*, cm^{-1}) 2921, 2851, 2598, 1607, 1579,1543, 1509, 1450, 1423, 1361, 1305, 1291, 1178, 1135, 1076, 1024, 826, 821,747. ^{1}H NMR (400 MHz, DMSO-d_6) δ 6.85 (s, 10H), 6.72 (dd, *J*= 5.8, 3.6 Hz, 2H), 6.59 (dd, *J*= 5.8, 3.6 Hz, 2H). ^{13}C NMR (101 MHz, DMSO-d_6) δ 145.7, 120.0 (bs), 119.7, 116.1.

Characterization

The molecular structure of the synthesized materials was examined by *Fourier-transform infrared spectroscopy (FT-IR)* using a Bruker Alpha-P spectrometer equipped with an ATR accessory (Wismar, Germany) in the range of 400–4000 cm^{-1}. *UV-Vis absorption spectra* were recorded for solutions of the substance in dimethyl sulfoxide (DMSO) using a Shimadzu UV-2600 spectrophotometer (Japan).

Liquid *NMR spectra* (^{1}H-, ^{13}C-, ^{13}C^{1}H-HSQC, ^{13}C^{1}H-HMBC, ^{15}N^{1}H-HSQC, ^{15}N^{1}H-HMBC experiments) were recorded for 2% solutions in DMSO-d_6 at 400 MHz on either a Bruker Avance III (Bruker, Rheinstetten, Germany) or a Bruker Avance Neo (Bruker, Ettlingen, Germany). Chemical shifts (δ) are reported in parts per million (ppm) relative to the deuterated solvent peaks, with the signal centre as the reference.

MALDI-TOF mass spectra were acquired using a Bruker RapifleX MALDI-TOF/TOF instrument (Bruker Daltonics, Bremen, Germany) equipped with a Smartbeam 3D laser, operating in positive reflectron ionization mode (RP). Samples were initially dissolved in DMSO and subsequently diluted (1:9, v/v) with acetonitrile to ensure a final DMSO content below 10%, minimizing signal suppression effects. Due to limited solubility, samples were only partially dissolved. The analytes were mixed with 2,5-dihydroxybenzoic acid (DHB) as matrix in a 1:2 (sample: matrix) ratio, deposited onto a MALDI target plate, and allowed to dry prior to analysis. Mass spectra were recorded in the m/z range of 100–3200 Da. Spectra were acquired both as individual sample spectra and as overlays with the matrix spectrum to facilitate identification and exclusion of matrix-related signals.

The thermal stability of the polymer was investigated by *thermogravimetric analysis (TGA*) and differential scanning calorimetry (DSC), performed on a STA 6000 (Perkin Elmer Instruments, USA) under a nitrogen flow (20 cm^3min^{-1}) over the temperature range from 25°C to 800°C at a heating rate of 10°C·min^{-1}. The *X-ray diffraction (XRD) patterns* were obtained with a Bruker AXS D8 Advance diffractometer (Wismar, Germany). The samples were mounted on conductive carbon tape and coated with a 20-nm layer by direct-current sputtering. To analyse the morphology of the nanocomposites, *Scanning Electron Microscopy*

(SEM) images were obtained using a Field Emission JEOL SEM 7001F (Tokyo, Japan) in *secondary electron imaging* (SEI) mode. Samples containing free radicals A (1) in the polycrystalline state were studied by *electron spin resonance* (ESR) at room temperature using a SE/X-2544 EPR spectrometer. The microwave frequency used was 9.4 GHz. The *electrical conductivity* of the oligomer was measured using a Keysight B2910BL source/measure unit (SMU) and applying a voltage of 42 V to each investigated sample. Ultrasonic Homogenizers and ultrasonic emulsification device probe sonicators (FS3N140303, 100 W, 40 Hz, manufactured in the USA) have been used in polymer synthesis to enhance reaction rates through cavitation induced by ultrasonic energy. This cavitation leads to the formation and collapse of tiny bubbles, thereby affecting solubility, diffusivity, penetration, and monomer transport in the medium.

Results and discussion

FT-IR analysis

The FT-IR spectrum of the synthesized compound *via* Method A is presented in Figure 1 (red curve). A broad absorption band in the 3550–2585 cm^{-1} region results from overlapping O–H (centred near 3350 cm^{-1}) and N–H (around 3218 cm^{-1}) stretching vibrations, both attributed to hydrogen-bonded functional groups that suggest intermolecular hydrogen bonding. The absorption peak at 3016 cm^{-1} corresponds to aromatic (C–H) stretching, while bands at 1564 and 1506 cm^{-1} are assigned to benzenoid (C–C) ring stretching. The 1285–1346 cm^{-1} region exhibits aromatic amine (C–N) stretching bands, and the 1168 cm^{-1} band is attributed to C–O stretching in phenolic groups. Bands at 819 and 715 cm^{-1} indicate out-of-plane C–H deformation in isolated and adjacent aromatic C–H groups. Collectively, these FT-IR signals support the formation of PPD–catechol co-oligomers. The absence of an intense absorption band characteristic of carbonyl groups in the region of 1690–1750 cm^{-1} supports the assumption that catechol is present predominantly in the phenolic rather than quinonoid form.

The FTIR spectrum of the sample obtained by Method B (Figure 1, blue curve) differs significantly from that of sample A, further confirming the formation of materials with different compositions. In the spectrum of sample B, the absorption band at 3218 cm^{-1} and the group of intense bands in the 1200–1400 cm^{-1} region, characteristic of amino groups, are absent. At the same time, more intense signals are observed in the 1000–1200 cm^{-1} region, which are attributed to C–O single-bond stretching vibrations. This observation supports the assumption that, under the experimental conditions of Method B, polycatechol is formed.

NMR analysis

To elucidate the structure of the surfactant- containing samples, NMR spectra were analysed for samples prepared in the presence of ethanol (Method B), which reduces protonation of aromatic amino groups. Under standard acidic conditions (Method C), signal broadening, presumably due to the formation of corresponding cations, decreases spectral resolution and complicates quantitative analysis. However, the positions of the peaks in the ^{1}H NMR spectra remain visually unchanged. This effect does not influence the quality of the ^{13}C NMR spectra.

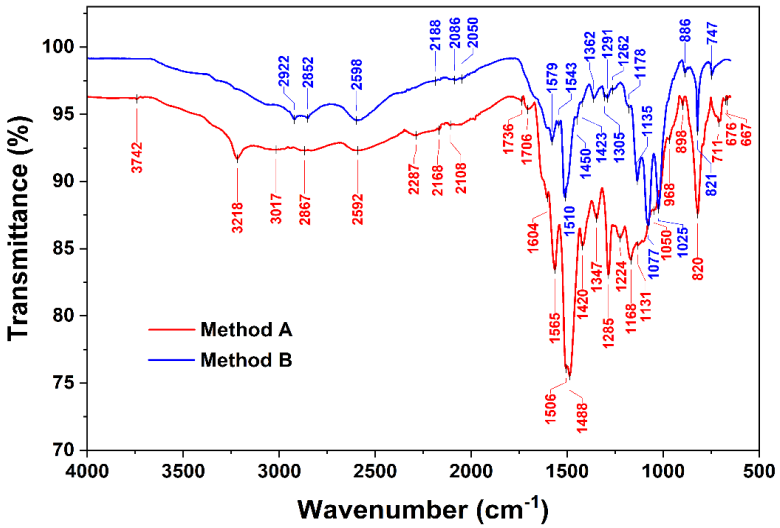

Figure 1. FT-IR absorption spectrum of oligo-(PPD–co-1,2-BD) obtained *via* Method A and Method B.

Thus, in the ^{1}H NMR spectrum (Figure 2*(a)*), signals are observed in the upfield region corresponding to the surfactant, dodecyl amine, while several groups of signals appear in the downfield region. Signals at 6.72 and 6.59 ppm (dd) are characteristic of the aromatic *ortho*- substituted fragment attributed to 1,2- dihydroxybenzene. A singlet at 6.85 ppm is also present. The integral ratio of the doublet of doublets to this singlet is 1:1:5, respectively. An intense broadened signal at 7.69 ppm is also observed, most likely corresponding to the protonated amino group of the surfactant, as confirmed by COSY spectra (Figure S1, Supplementary material), where a cross-peak with methylene protons adjacent to nitrogen (2.76 ppm) is detected. Additionally, low- intensity singlets at δ 9. 24 and 5. 68 ppm are present, which are characteristic of dione structure **1** (Figure 3), corresponding to an oxidized and substituted 1,2- dihydroxybenzene. The signal at 9.24 ppm is attributed to an amino group. Literature reports indicate that secondary amine protons may appear in this region [43]. The signal at 5.68 ppm corresponds to a CH group of this fragment. To determine whether this fragment is connected to the oligomer molecule, additional one- and two- dimensional NMR spectra were analysed. Due to the low content of this fragment, the ^{13}C NMR (Figure 2*(b)*) and HSQC (Figure S2) spectra do not provide sufficient information for structural conclusions. However, in the HMBC spectrum (Figure S3), cross-peaks for these signals are observed at approximately 180 ppm and 150.4 ppm, values characteristic of carbons adjacent to hydroxyl and amino groups in such kind of molecules [43], respectively.

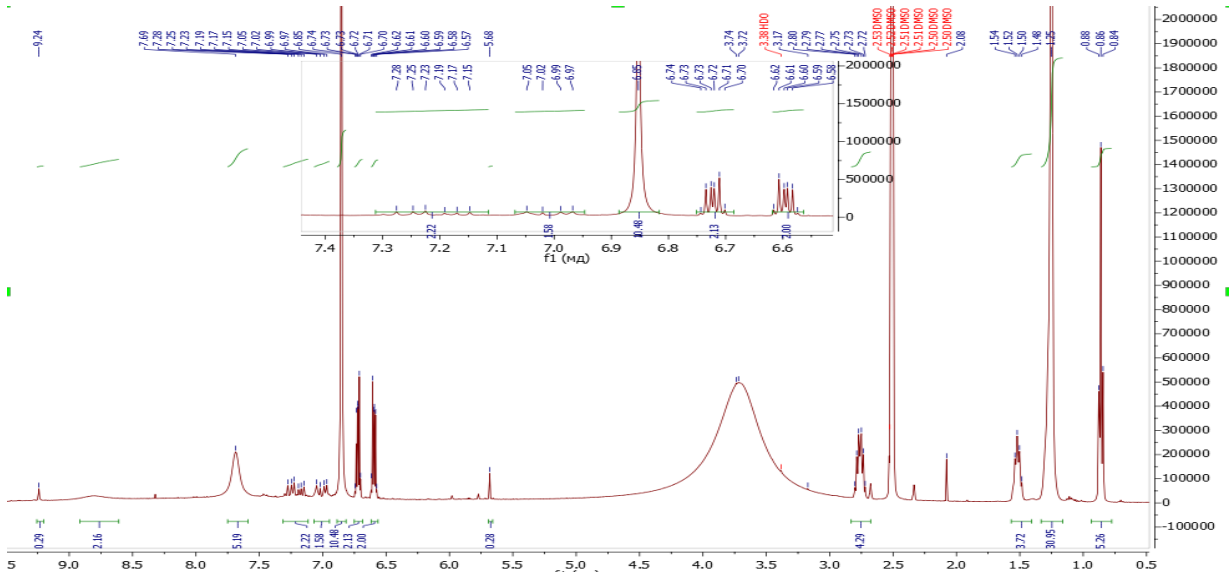

(a)

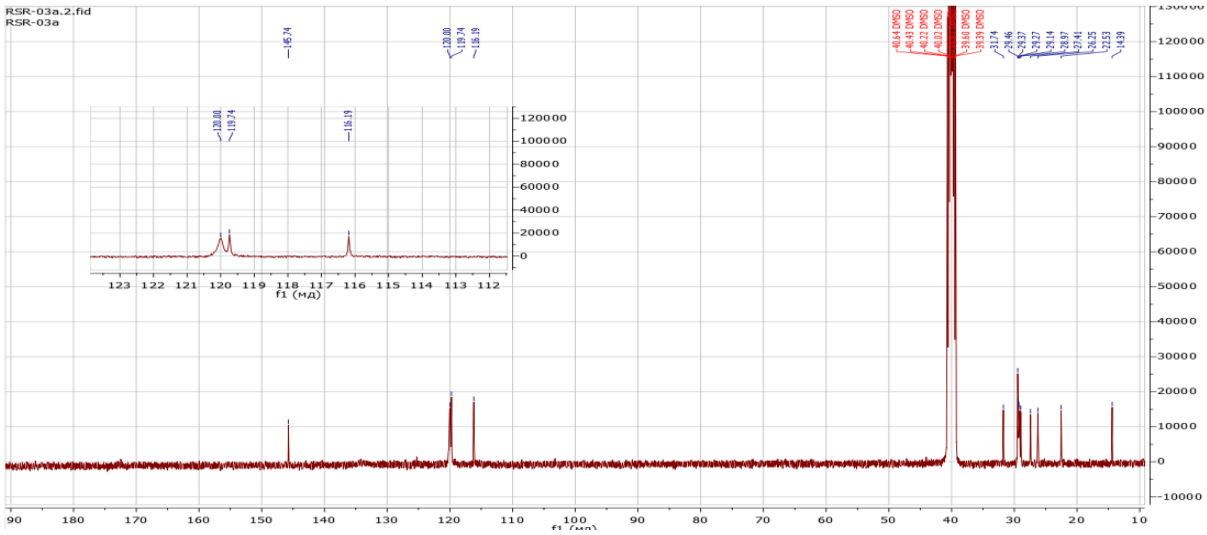

(b)

Figure 2. The ^{1}HNMR *(a)* and ^{13}CNMR *(b)* spectrum of oligo-(PPD–co-1,2-BD) in DMSO-d_6.

It was observed that when oxidative polycondensation is carried out without ethanol (Method C), the resulting product shows a fourfold increase in the ratio of the trimer fragment proton integrals relative to the rest of the molecule. This enables the detection of minor signals in the ^{13}C spectrum and their assignment to the discussed fragment. Thus, in the ^{13}C NMR spectrum (Figure S4), signals appear at 179.1, 148.7, 115.7, and 94.3 ppm, and the intensity of the signal at 125.3 ppm increases significantly. According to DEPT data (Figure S5), the signals at 125.3, 115.7, and 94.3 ppm correspond to CH groups. The latter signal is particularly characteristic and can be clearly attributed to the CH group of the catechol fragment of trimer **1**. The remaining CH signals correspond to protons in the 2,6- and 3,5-positions of the *para*-phenylenediamine ring. These protons in the ^{1}H NMR spectrum (Figure 2*(a)*) give multiple signals in the region of 7.30–6.97 ppm, which is further confirmed by weak cross-peaks in the HSQC spectrum (Figure S2). At the same time, no correlations between this structure and other fragments are observed in the HMBC spectra (Figure S3). All of this data confirms the formation of the compound **1** (Figure 3) in the reaction mass.

As a next step to confirm the proposed structure, elemental analysis was performed to determine the carbon-to-nitrogen ratio. For this purpose, the synthesis was carried out under oxidative polycondensation conditions in an acidic aqueous medium without a surfactant (Method A). However, the resulting sample consisted predominantly of compound **1** with a minor amount of compound **2**, as indicated by the integral intensities in the ^{1}H NMR spectrum (Figure S6).

Similarly, the data corresponding to the remaining signals were analysed to elucidate the structure of the second component in the sample mixture. Analysis of the HMBC data (Figure S3) shows that the aromatic protons of the terminal *ortho*-dihydroxy benzene unit correlate with a quaternary carbon at 145.7 ppm, which is typical for a carbon atom bonded to a hydroxyl group in such systems. In turn, the singlet protons at 6.85 ppm correlate only with carbons resonating at around 119 ppm, indicating overlap among multiple signals with very similar chemical shifts. Such a result is only possible if these protons are nearly equivalent.

Based on these data, it was assumed that the second compound formed in the reaction medium under oxidative polymerization conditions in the presence of a surfactant and ethanol (Method B) is poly(*ortho*-dihydroxybenzene) with structure **2** (Figure 3). The integral value of 2 for each doublet of doublets at 6.60 and 6.72 ppm was assigned, assuming that a linear molecule contains one terminal *ortho*-fragment. Accordingly, the singlet at 6.98 ppm has an integral value of 10, corresponding to five 1,2-dihydroxybenzene units.

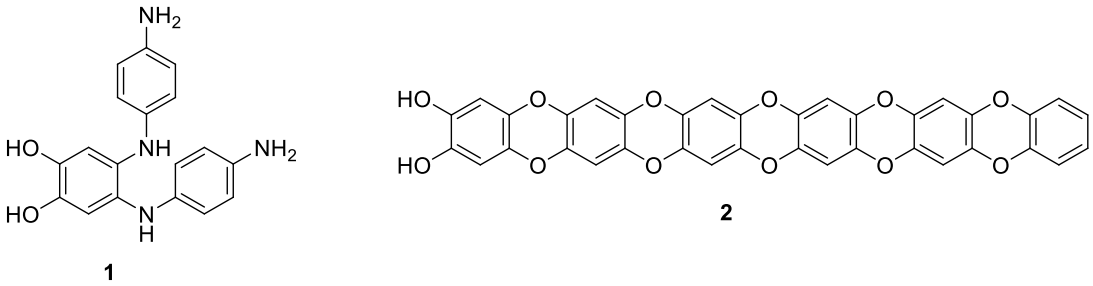

Figure 3. Oligomers obtained *via* oxidative polycondensation of *p*-phenylenediamine and catechol.

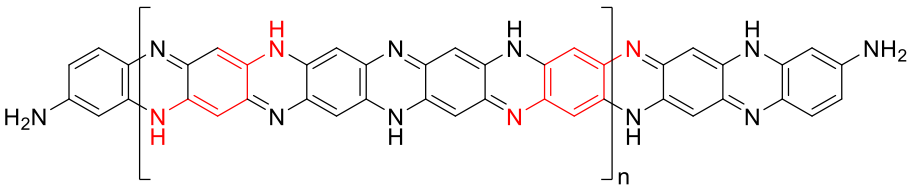

Figure 4. Product obtained *via* oxidative polycondensation of *p*-phenylenediamine in the presence of DDA.

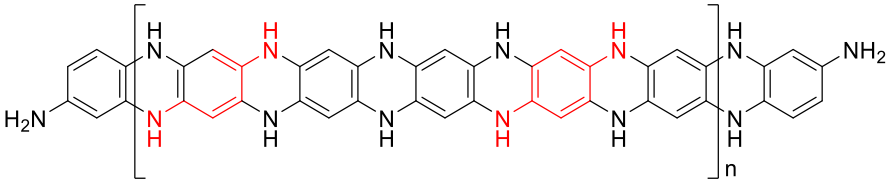

Figure 5. Product obtained *via* oxidative polycondensation of *p*-phenylenediamine without DDA.

It is worth noting that numerous examples of polycondensation of *para*-phenylenediamine have been reported in the literature, even under similar conditions [45-47], with different product structures and mechanisms proposed. To exclude the formation of poly(*para*-phenylenediamine), the polycondensation was carried out under identical conditions but without 1,2-dihydroxybenzene. However, in this case, a completely different product was obtained, as confirmed by comparison of the spectral data with those of samples prepared in the absence of 1,2-dihydroxybenzene. When a surfactant was used, the product exhibited a doublet in the ^{1}H NMR spectrum (Figure S7), characteristic of conjugated protons, and three signals in the ^{13}C NMR spectrum (Figure S8) at 149.2, 126.3, and 114.6 ppm, which is consistent with the structure of poly(*para*-phenylenediamine) shown in Figure 4 and agrees with literature data [46].

When the reaction was performed without a surfactant, the obtained product showed only one CH signal at 7.28 ppm in the ^{1}H NMR spectrum (Figure S9) and two signals in the ^{13}C NMR spectrum at 120.1 and 134.8 ppm, which may correspond to the structure presented in Figure 5. Such a structure has not been reported in the literature to the best of our knowledge. It should also be noted that detailed NMR studies of such systems are scarce, which limits a full comparative analysis.

Thus, it was demonstrated that the target product is not a result of polycondensation of *para*-phenylenediamine. The absence of nitrogen is further supported by the lack of cross-peaks in the ^{15}N^{1}H-HMBC spectrum.

To verify the assumption that *ortho*-dihydroxy benzene can participate in such reactions, oxidative polycondensation was carried out in the absence of *para*-phenylenediamine. Under these conditions, a product was obtained whose ^{1}H NMR spectrum (Figure S10) exhibited signals similar to those observed in our case, namely a singlet and two doublets of doublets. However, the degree of polymerization was lower; according to the obtained data, dimers were predominantly formed. Nevertheless, the formation of such a structure confirms the validity of our assumption.

Thus, it can be concluded that 1,2-dihydroxy benzene, acts as an inhibitor of oxidative polymerization, yielding a trimer (structure **1**) that does not undergo further chain growth. This behaviour can be explained by the stability of the radical formed during the initiation step of radical polycondensation, which results in delocalization across the entire conjugated system. Consequently, this stabilization renders the trimer unreactive toward further propagation. The use of a surfactant in an acidic aqueous medium lead to the formation of a mixture of compounds **1** and **2** in approximately a 1:1 ratio. The addition of an organic solvent (ethanol) further increases the content of compound **2,** reaching a ratio of compounds 1:2 = 1:4 under the described conditions.

MALDI-TOF MS analysis.

Figure 6*(b)* presents the MALDI-TOF mass spectrum in comparison with the reference spectrum Figure 6*(a)*. A signal at m/z 649.565 is observed, which correlates with the expected values for protonated polycatechol species (theoretical molecular weight ~640 Da).

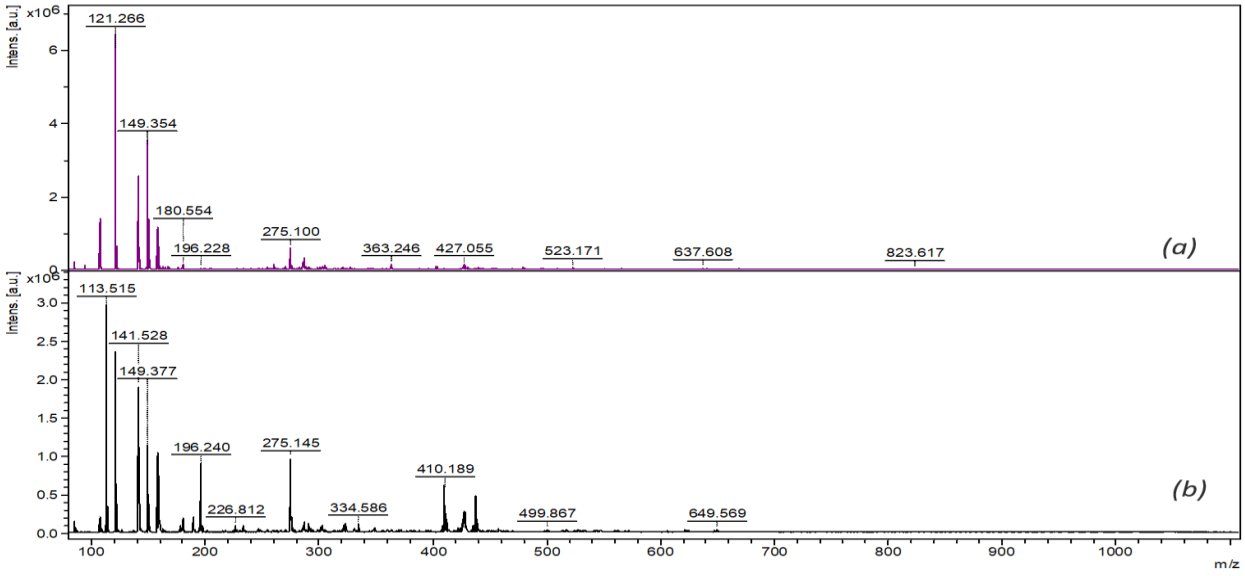

Figure 6. The MALDI-TOF mass spectrum of reverence DHB *(a)* and the MALDI-TOF mass spectrum of the sample in comparison with the reference spectrum of DHB *(b)*.

Additionally, signals in the m/z range of 322 are detected, which can be attributed to the presence of trimer. The relatively low intensity of the observed peaks is consistent with the low concentration of the analyte in the sample.

The proposed mechanisms for the formation of compounds **1** and **2** are presented in Schemes 1 and Scheme 2, respectively. Upon interaction of the sulfate radical anion with a catechol molecule, homolytic abstraction of a hydrogen atom from one of the hydroxyl groups occurs, resulting in the formation of a radical species characterized by several resonance structures, among which structure **I** is considered the most stable. This intermediate subsequently reacts with a *para*-phenylenediamine molecule to form intermediate **II**, which undergoes enolization to yield intermediate **III**. Further interaction of the latter with a *para*-phenylenediamine-derived radical leads to the formation of compound **1**.

In the presence of a surfactant, competing interactions involving amino-containing compounds in the reaction medium appear to occur. Alternatively, dodecyl amine may preferentially surround *para*-phenylenediamine molecules through hydrogen-bonded associations, thereby reducing their reactivity. In contrast, catechol tends to form intramolecular hydrogen bonds between its two hydroxyl groups and is therefore less susceptible to interaction with the surfactant. As a consequence, due to the reduced reactivity of *para*-phenylenediamine, the radical intermediate **I** preferentially reacts with a second catechol molecule (Scheme 2), leading to the formation of intermediate **IV**, which is subsequently converted into intermediate **V**. Further oxidation results in the formation of dimer **VI**. Subsequent chain growth proceeds through the addition of radical **I** to the growing polymer chain.

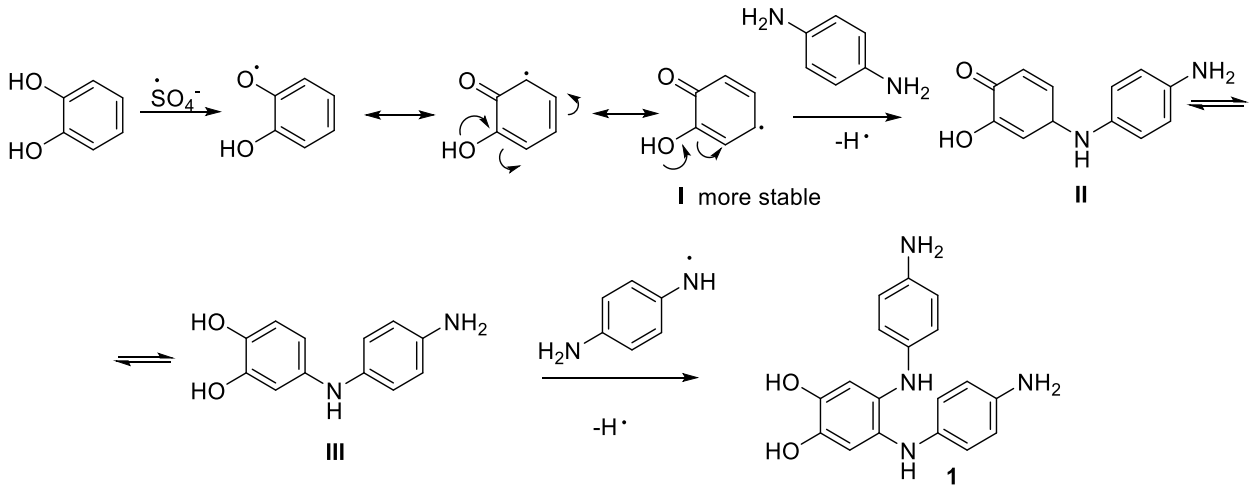

Scheme 1. Proposed mechanism for the formation of compound 1.

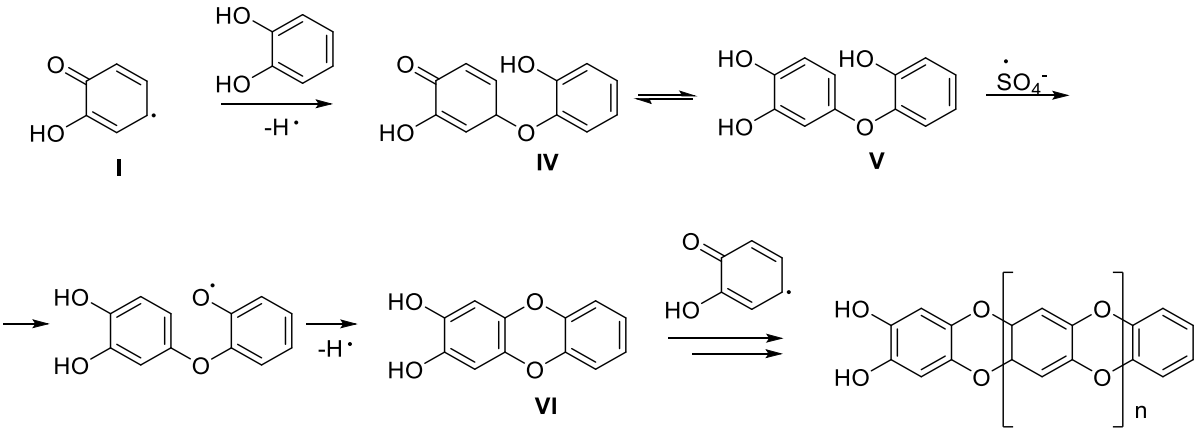

Scheme 2. Proposed mechanism for the formation of compound 2.

UV-Vis spectroscopy

UV-Vis spectroscopy was employed to assess the optical and electronic properties of the synthesized compound. As shown in Figure 7, the synthesized aromatic oligomer reveals a highly conjugated electronic structure with a distinct optical band gap. Intense π→π* transitions in the deep-UV region (200–260 nm) confirm the preservation of the aromatic backbone following polymerization. Additionally, the presence of a pronounced absorption shoulder attributed to n→π* transitions (280–350 nm), together with a broad visible-light peak centred at 450 nm, indicates effective chain growth and the development of an extended conjugated system involving the lone pairs of nitrogen and oxygen atoms. The optical band gap was estimated using Tauc plot analysis (inset in Figure 7) and was found to be approximately 4.7 eV. This value suggests that the obtained material behaves as a wide-band-gap organic semiconducting system. The observed optical response reflects the influence of the conjugated aromatic framework together with the presence of heteroatom-containing functional groups formed during oxidative polycondensation.

Thermogravimetric analysis

Thermal degradation of the sample was examined by thermogravimetric analysis (TGA), as shown in Figure 8. The graph shows a multi-step weight-loss, indicating distinct thermal degradation processes. The initial weight loss ≈ 3.5% observed bellow 150°C is attributed to the removal of adsorbed water and residual solvent molecules. The main degradation step occurs in the most critical region around 260–300°C, with a significant mass loss of about 39.5%. This process is associated with the decomposition of the oligomeric linkage or the loss of a smaller, low-molecular-weight oligomeric fraction, as evidenced by the peak in the derivative thermogravimetric (DTG) curve centred at approximately 300°C ($DTG_{max} \approx -8$%/min).

Beyond 350°C, a gradual mass loss of approximately 17% is observed up to 700°C, corresponding to the further degradation and carbonization of the conjugated backbone. The material retains a relatively high residual mass of about 40% at 700°C, indicating enhanced thermal stability. Overall, the observed thermal behavior is consistent with previously reported aromatic amine–based conductive oligomers [48,49], suggesting that the synthesized materials exhibit moderate thermal stability and may be promising for electronic applications.

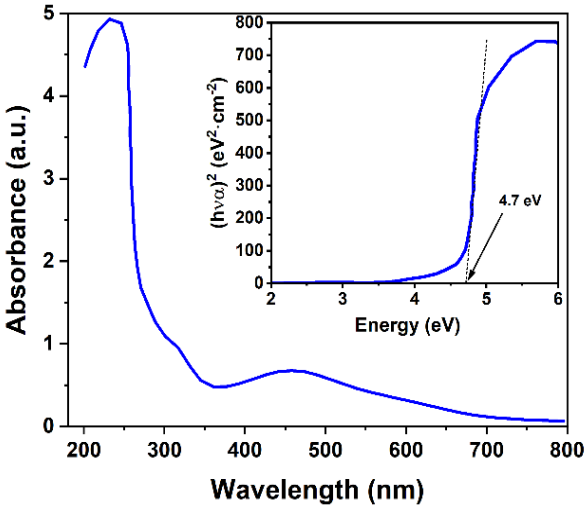

Figure 7. UV-Vis spectrum of oligo-(PPD–co-1,2-BD).

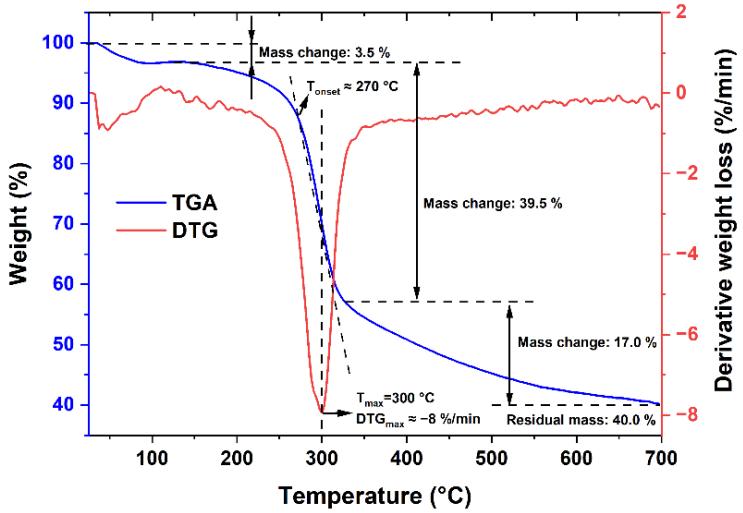

Figure 8. Temperature dependence of the weight loss of oligo-(PPD–co-1,2-BD) (blue) and DTG (red) curves during heating up to 700 °C at a rate of 10 °C/min.

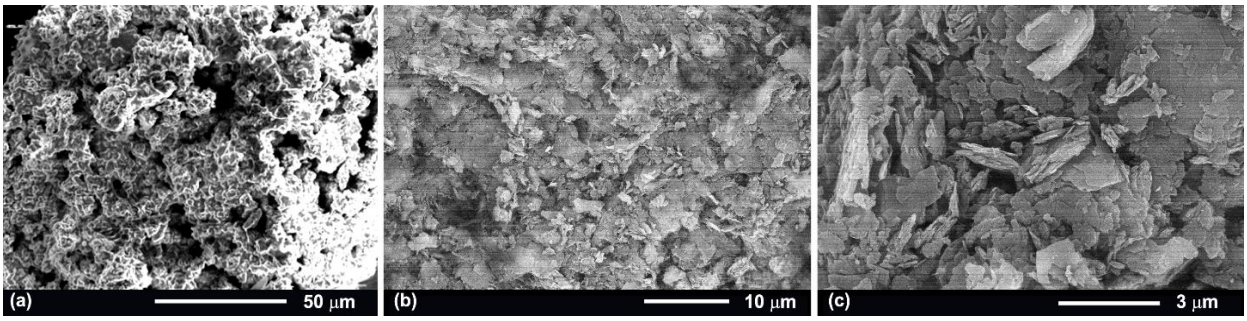

(a) *(b)* *(c)*

Figure 9. SEM micrographs of oligo-(PPD-co-1,2-BD) recorded at different magnifications, showing the evolution from compact aggregated domains *(a)* to irregular flake-like and partially stacked structural assemblies at higher magnification *(b,c)*.

Scanning electron microscopy

The SEM images (Figure 9) reveal that the synthesized oligo-(PPD-co-1,2-BD) exhibits a non-uniform and highly textured morphology. At lower magnification, the material appears as compact aggregates with an interconnected domain. At higher magnification, the surface is composed of irregular fragments combining predominantly flake-like features. No well-defined individual particles can be distinguished, suggesting that the copolymerization process promotes the formation of interconnected domains rather than discrete entities. This morphology can be associated with the conditions imposed by ultrasound-assisted oxidative synthesis, where rapid nucleation and continuous growth lead to the formation of partially stacked and compact structural assemblies. Such structural characteristics may enhance surface accessibility and contribute to improved performance in applications involving interfacial processes.

X-ray diffraction (XRD) analysis

X-ray diffraction (XRD) analysis reveals a pattern characterized by several sharp diffraction peaks superimposed on a broad diffuse halo. The presence of relatively sharp reflections suggests the existence of ordered structural domains within the synthesized material, while the diffuse contribution indicates the coexistence of disordered regions typical for oligomeric systems. The most intense reflection observed at approximately $2\theta \approx 9°$, together with the group of peaks between 18° and 25°, may be associated with intermolecular organization promoted by hydrogen bonding and π–π interactions between aromatic fragments. At the same time, the broad diffuse contribution in the 15°–30° region suggests that the material does not possess complete long-range crystallinity. Overall, the XRD results indicate partial structural ordering within the oligomeric matrix (Figure 10).

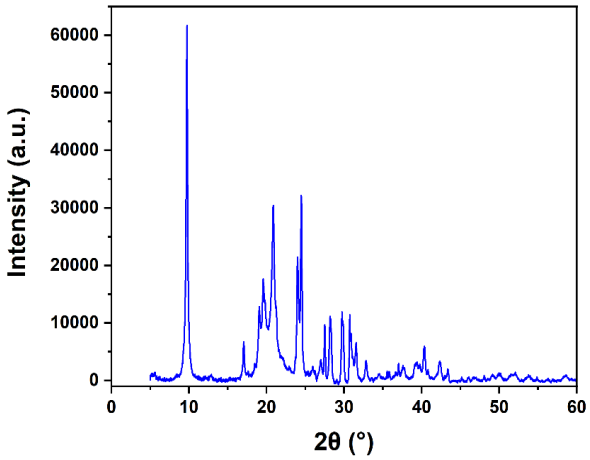

Figure 10. XRD patterns of oligo-(PPD–co-1,2-BD).

ESR analysis

The ESR spectrum (Figure S11) of the synthesized co-oligomer (PPD-co-1,2-BD), measured in the X-band at room temperature, exhibits a single resonance line with a g-factor of 2.0039 ± 0.0005 and a peak-to-peak linewidth ΔBpp= (1.69 ± 0.08) mT. The g-factor for co-oligomer practically matches that of the standard radical 2,2-diphenyl-1-picrylhydrazyl (DPPH), g= 2.0036 [50], indicating that the unpaired electrons in the co-oligomer and DPPH are in a similar magnetic environment. In contrast, the ΔBpp of the co-oligomer is approximately 18,8 times greater than the 0.09 mT observed for DPPH using 1.1-GHz continuous wave ESR spectroscopy with a frequency modulation method [51]. This broader ESR line indicates substantially weaker exchange interactions in the co-oligomer in comparison with DPPH.

Conductivity

Oligo-(PPD-co-1,2-BD) nanocomposites synthesized in different methods (A, B, and C), both with and without surfactants demonstrated unconventional electrical behaviour when

evaluated using a Keysight B2910BL source/measure unit (SMU) and applying a voltage of 42 V to each investigated sample. Unlike typical semiconductors, where conductivity increases with temperature, the conductivity of this compound increased as temperature decreased (Figure 12). The measured conductivity at room temperature was 1.06 × 10^{-7} S/cm, highlighting the material's distinctive temperature-dependent properties.

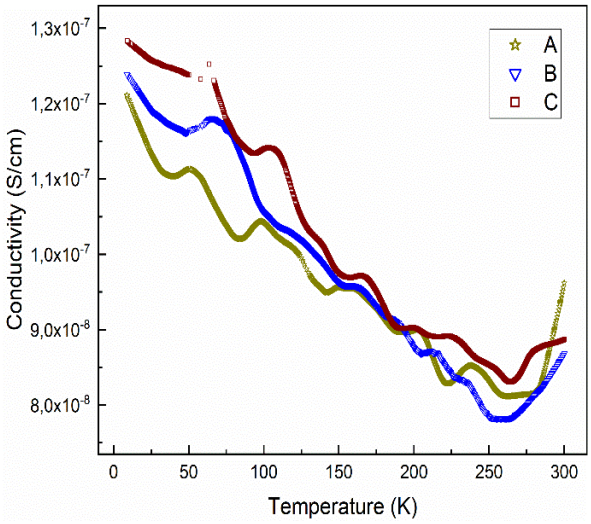

Figure 12. Temperature-dependent conductivity diagram of the oligo-(PPD-co-1,2-BD).

Conclusions

Oligomeric materials based on *p*-phenylenediamine and 1,2-benzenediol were synthesized in different media, both with and without surfactant. This was achieved *via* oxidative polymerization under ultrasonic irradiation, employing a 1:1 monomer-to-PPS ratio at 0–15°C for 8 hours.

Comprehensive structural and morphological characterization was conducted using FT-IR, ^{1}H and ^{13}C NMR, UV-Vis, TGA, SEM, XRD, and ESR spectroscopy. FT-IR and NMR analyses confirmed the formation of both co-oligomer and homo-oligomer of 1,2-benzenediol. Reaction conditions determine product distribution: oxidized 1,2-dihydroxy benzene limits chain growth by stabilizing radicals and favouring trimer formation, whereas medium composition further modulates outcomes. Notably, the presence of surfactant and ethanol increases the yield of oligo-1,2-benzenediol, highlighting the importance of these factors in guiding product selectivity.

UV-Vis spectroscopy demonstrated that, despite radical localization, sufficient conjugation and electronic interactions are present to produce a significant optical band gap, classifying the material as an organic semiconductor. TGA results indicated moderate thermal stability up to 270°C. SEM observations revealed heterogeneous aggregated structures composed predominantly of irregular flake-like domains, while XRD analysis suggested partial structural ordering within the oligomeric matrix. ESR spectroscopy verified the presence of stable, localized radicals with weak exchange interactions. The electrical conductivity, measured by the four-probe method, was 1.06 × 10^{-7} S/cm. In addition, the presence of polar functional groups (–NH-) enhanced solubility in common polar organic solvents such as DMSO and DMF.

Funding

This research was supported by the Moldovan National Agency for Research and Development (Project Nr. 25.80012.5007.72SE).

Supplementary information

Supplementary data are available free of charge at http://cjm.ichem.md as PDF file.

References

1. Li, X.-G.; Huang, M.-R.; Duan, W.; Yang, Y.-L. Novel multifunctional polymers from aromatic diamines by oxidative polymerizations. Chemistry Review, 2002, 102(9), pp. 2925–3030. DOI: https://doi.org/10.1021/cr010423z
2. Babel, V.; Hiran, B.L. A review on polyaniline composites: synthesis, characterization and applications. Polymer Composite, 2021, 42(7), pp. 3142–3157. DOI: https://doi.org/10.1002/pc.26048
3. Qiu, H.; Zhao, X.; Li, H.; Li, Y.; Li, J.; Yang, J. Highly flexible and thermal conductive films of graphene/poly(naphthylamine) and applications in thermal management of LED devices. Journal of Applied Polymer Science, 2021, 138(46), 51383, pp. 1–10. DOI: https://doi.org/10.1002/app.51383
4. Travis, A.S. Anilines: historical background. Patai, S.; Rappoport, Z. Eds. The Chemistry of Anilines. John Wiley & Sons, 2007, pp. 1–73. https://doi.org/10.1002/9780470871737.ch1
5. Sapurina, I.Yu.; Shishov, M.A. Oxidative Polymerization of Aniline: Molecular Synthesis of Polyaniline and the Formation of Supramolecular Structures. De Souza Gomes, A. Ed. New Polymers for Special Applications. IntechOpen: London, 2012, pp. 252–312. DOI: https://doi.org/10.5772/48758
6. Noelting, E. Scientific and Industrial History of Aniline Black. Matheson & Co.: New York, 1889, 165 p.
7. Stejskal, J.; Hlavatá, D.; Holler, P.; Trchová, M.; Prokeš, J.; Sapurina, I. Polyaniline prepared in the presence of various acids: conductivity study. Polymer International, 2004, 53(3), pp. 294–300. DOI: https://doi.org/10.1002/pi.1406

8. Scott, J.C. History of Conductive Polymers. Eftekhari, A. Ed. Nanostructured Conductive Polymers. John Wiley & Sons, 2010, pp. 1–17. DOI: https://doi.org/10.1002/9780470661338.ch1
9. Gupta, A.; Kumar, M. Optical and structural properties of chromium (Cr) doped polyaniline. International Journal of Research in Advent Technology, 2019, 7(3), pp. 1232–1234. DOI: https://doi.org/10.32622/ijrat.73201994
10. Azzouz, A.; Vikrant, K.; Kim, K.-H.; Ballesteros, E.; Rhadfi, T.; Malik, A.K. Advances in colorimetric and optical sensing for gaseous volatile organic compounds. TrAC Trends in Analytical Chemistry, 2019, 118, pp. 502–516. DOI: https://doi.org/10.1016/j.trac.2019.06.017
11. Kuramoto, N.; Genies, E.M. Micellar chemical polymerization of aniline. Synthetic Metals, 1995, 68(2), pp. 191–194. DOI: https://doi.org/10.1016/0379-6779(94)02284-6
12. Karg, S.; Scott, J.C.; Salem, J.R.; Angdopoulos, M. Increased brightness and lifetime of polymer light-emitting diodes with polyaniline anodes. Synthetic Metals, 1996, 80(2), pp. 111–117. DOI: https://doi.org/10.1016/S0379-6779(96)03690-9
13. Beygisangchin, M.; Abdul Rashid, S.; Shafie, S.; Sadrolhosseini, A.R.; Lim, H.N. Preparations, properties, and applications of polyaniline and polyaniline thin films - A review. Polymers, 2021, 13(12), 2003, pp. 1–46. DOI: https://doi.org/10.3390/polym13122003
14. Get, R.; Islam, S.M.; Singh, S.; Mahala, P. Organic polymer bilayer structures for applications in flexible solar cells devices. Microelectronic Engineering, 2020, 222, 111200, pp. 1–6. DOI: https://doi.org/10.1016/j.mee.2019.111200
15. Itoi, H.; Hayashi, S.; Matsufusa, H.; Ohzawa, Y. Electrochemical synthesis of polyaniline in the micropores of activated carbon for high-performance electrochemical capacitors. Chemical Communications, 2017, 53(22), pp. 3201–3204. DOI: https://doi.org/10.1039/C6CC08822H
16. Lakard, B. Electrochemical biosensors based on conducting polymers: A review. Applied Sciences, 2020, 10(18), 6614, pp. 1–24. DOI: https://doi.org/10.3390/app10186614
17. Chen, C.; Gan, Z.; Xu, C.; Lu, L.; Liu, Y.; Gao, Y. Electrosynthesis of poly(aniline-co-azure B) for aqueous rechargeable zinc-conducting polymer batteries. Electrochimica Acta, 2017, 252, pp. 226–233. DOI: https://doi.org/10.1016/j.electacta.2017.08.195
18. Yano, J.; Nakatani.; Harima, Y.; Kitani A. Bilayer polymer coating containing a polyaniline for corrosion protection of iron. 2007, 61(7), pp.1500–1503. DOI: https://doi.org/10.1016/j.matlet.2006.07.061
19. Mamatha, G.M., Pradipkumar, D.; Krishna, R.H.; Kumar, K.S. Polymer based composites for electromagnetic interference (EMI) shielding: The role of magnetic fillers in effective attenuation of microwaves, a review. Hybrid Advances, 2024, 6, pp. 100200. DOI: https://doi.org/10.1016/j.hybadv.2024.100200
20. Rzayev, R.S.; Mammadov, B.A.; Abdullayev, Y.A.; Ibadov, E.A. Synthesis of characterization of new nano-sized poly(*p*-phenylenediamine) in the presence of potassium persulfate. Processes of Petrochemistry and Oil Refining, 2022, 23(3), pp. 495–509.
21. Stejskal, J. Polymers of phenylenediamines. Progress in Polymer Science, 2015, 41, pp. 1–31. DOI: https://doi.org/10.1016/j.progpolymsci.2014.10.007
22. Nascimento, G.M.; Sestrem, R.M.; Temperini, M.L.A. Poly-*para*-phenylenediamine–montmorillonite clay nanocomposites. Synthetic Metals, 2010, 160 (23–24), pp. 2397–2403. DOI: https://doi.org/10.1016/J.SYNTHMET.2010.09.016
23. Huner, K. Synthesis, characterization, and thermoelectric properties of poly(*p*-phenylene diamine)/poly(sulfonic acid diphenyl aniline) composites. Polymer Engineering and Science, 2022, 62(8), pp. 2560–2568. DOI: https://doi.org/10.1002/pen.26041
24. Bláha, M.; Trchová, M.; Morávková, Z.; Humpolíček, P.; Stejskal, J. Semiconducting materials from oxidative coupling under various acidic conditions. Materials Chemistry and Physics, 2018, 205, pp. 423–435. DOI: https://doi.org/10.1016/j.matchemphys.2017.11.007
25. Olgun, U.; Gülfen, M. Doping of poly(*o*-phenylenediamine): Spectroscopy, voltammetry, conductivity and band gap energy. Reactive and Functional Polymers, 2014, 77, pp. 23–29. DOI: https://doi.org/10.1016/j.reactfunctpolym.2014.02.006
26. Chan, H.S.O.; Ng, S.C.; Hor, T.S.A.; Sun, J.; Tan, K.L.; Tan, B.T.G. Poly(*m*-phenylenediamine): Synthesis and characterization by X-ray photoelectron spectroscopy. European Polymer Journal, 1991, 27(11), pp. 1303–1308. DOI: https://doi.org/10.1016/0014-3057(91)90069-Z
27. Prokeš, J.; Stejskal, J.; Křivka, I.; Tobolková, E. Aniline-phenylenediamine copolymers. Synthetic Metals, 1999, 102(1-3), pp. 1205–1206. DOI: https://doi.org/10.1016/S0379-6779(98)01223-5
28. Amer, I. Sulfonation of poly(*p*-phenylene diamine) polymer. Cogent Engineering, 2017, 4(1), pp. 1329790. DOI: https://doi.org/10.1080/23311916.2017.1329790
29. Abdullayev, Y.; Rzayev, R.; Autschbach, J. Computational mechanistic studies on persulfate assisted *p*-phenylenediamine polymerization. Journal of Computational Chemistry, 2022, 43(19), pp. 1313–1319. DOI: https://doi.org/10.1002/jcc.26943
30. Amer, I.; Young D.A. Chemically oxidative polymerization of aromatic diamines: The first use of aluminium-triflate as a co-catalyst. Polymer, 2013, 54(2), pp. 505–512. DOI: https://doi.org/10.1016/j.polymer.2012.11.078
31. Su, J.; Fu, J.; Wang, Q. Laccase: a green catalyst for the biosynthesis of poly-phenols. Critical Reviews in

Biotechnology, 2018, 38, pp. 294–307. DOI: https://doi.org/10.1080/07388551.2017.1354353
32. Mamedov, B.A.; Shahnazarli R.Z.; Rzayev R.S.; Ishenko N.Ya.; Nazaraliev Kh.G.; Mamedov M.M.; Guliyev A.M. synthesis of oligohydroxynapthylenes and their use in making of heat-stable and electro-conducting rubbers. Journal of Chemistry and Chemical Engeneering, 2011, 5, pp. 832–840.
33. Nagamani, C.; Guo, J.; Thayumanavan, S. Synthesis and characterization of phenol-based biaryl proton conducting polymers. Journal of Polymer Science A Polymer Chemistry, 2012, 50(6), pp. 1187–1196. DOI: https://doi.org/10.1002/pola.25880
34. Nagarajan S.; Nagarajan R.; Kumar J.; Salemme A.; Togna A.R.; Saso L.; Bruno F. Antioxidant activity of synthetic polymers of phenolic compounds. Polymers, 2020, 12(8), pp. 1646. DOI: https://doi.org/10.3390/polym12081646
35. Reihmann, M., Ritter, H. Synthesis of Phenol Polymers Using Peroxidases. In: Kobayashi, S., Ritter, H., Kaplan, D. (eds) Enzyme-Catalyzed Synthesis of Polymers. Advances in Polymer Science, Springer, Berlin, Heidelberg, 2005, 194, pp. 1–49. DOI: https://doi.org/10.1007/12_034
36. Razaviamri, S.; Wang, K.; Liu, B.; Lee, B.P. Catechol-based antimicrobial polymers. Molecules, 2021, 26(3), pp. 559. DOI: https://doi.org/10.3390/molecules26030559
37. Faure, E.; Falentin-Daudré, C.; Jérôme, C.; Lyskawa, J.; Fournier, D.; Woisel, P.; Detrembleur, C. Catechols as versatile platforms in polymer chemistry. Progress in Polymer Science, 2013, 38(1), pp. 236–270. DOI: https://doi.org/10.1016/j.progpolymsci.2012.06.004
38. Yan G.; Chen G.; Peng Z.; Shen Z.; Tang X.; SunY.; Zeng X.; Lin L. The cross-linking mechanism and applications of catechol-metal polymer materials. Advanced Material Interfaces, 2021, 8(19), pp. 2100239. DOI: https://doi.org/10.1002/admi.202100239
39. Zhang, H.; Zhao T.; Newland B.; Liu W.; Wang We.; Wang W. Catechol functionalized hyperbranched polymers as biomedical materials. Progress in Polymer Science, 2018, 78, pp. 47–55. DOI: https://doi.org/10.1016/j.progpolymsci.2017.09.002
40. Lee, B.P.; Birkedal, H.; Lee, H. Editorial: Catechol and polyphenol chemistry for smart polymers. Frontiers in Chemistry, 2019, 7, pp. 883. DOI: https://doi.org/10.3389/fchem.2019.00883
41. Abdelwahab, N.A.; Al-Ashkar, E.A.; El-Ghaffar, M.A. ABD. Preparation and characterization of eco-friendly poly(*p*-phenylenediamine) and its composite with chitosan for removal of copper ions from aqueous solutions. Transactions of Nonferrous Metals Society of China, 2015, 25(11), pp. 3808–3819. DOI:10.1016/S1003-6326(15)64025-0
42. Badawi, H.M.; Förner, W.; Ali, S.A. A comparative study of the infrared and Raman spectra of aniline and *o*-, *m*-, *p*-phenylenediamine isomers. Spectrochim. Acta Part A, Molecular and Biomolecular Spectroscopy, 2013, 112, pp. 388–396. DOI: https://doi.org/10.1016/j.saa.2013.04.07
43. Rzayev, R.; Sucman, N.; Geru, I.; Monaico, E.; Mammadov, B.; İbadov, E.; Macaev, F. Synthesis and characterization of nano-sized materials based on toluidine and resorcinol. ChemistrySelect, 2025, 10(22), pp. e01279. DOI: https://doi.org/10.1002/slct.202501279
44. Rzayev, R.; Sucman, N.; Geru, I.; Monaico, E.; Nicolescu, A.; Mammadov, B.; Deleanu, C.; İbadov, E.; Macaev, F. Multifunctional thermostable oligomer based on *para*-phenylenediamine and resorcinol with hierarchical micro- and submicron structure. Journal of Polymer Research, 2026, 33, pp. 243. DOI: https://doi.org/10.1007/s10965-026-04966-8
45. Zaitsev, B. A.; Kleptsova, L. G.; Shvabskaya, I. D.; Bursian A. Thermo-oxidative oligomerization of aromatic diamine. Organic Polymer Material Research, 2021, 3(1), pp. 24-31. DOI: https://doi.org/10.30564/opmr.v3i1.3612
46. Cataldo, F. On the polymerization of *P*-phenylenediamine. European Polymer Journal, 1996, 32(1), pp. 43–50. DOI: https://doi.org/10.1016/0014-3057(95)00118-2
47. Durgaryan A. A.; Arakelyan R. A.; Durgaryan, N. A. Oxidative polymerization of *p*-phenylene diamine. Russian Journal of General Chemistry, 2014, 84, pp. 1095–1100. DOI: https://doi.org/10.1134/S1070363214060073
48. Liou G.-Sh.; Lin, H.-Y. Electrochemical and electrochromic properties of novel aromatic poly(amine-amide)s derived from *N,N′*-bis(4-carboxyphenyl)-*N,N′*-diphenyl-1,4-phenylenediamine. European Polymer Journal, 2006, 42(5), pp. 1051-1058. DOI: https://doi.org/10.1016/j.eurpolymj.2005.11.022
49. Hsiao, S.-H.; Lu, H.-Y. Electrosynthesis of aromatic poly(amide-amine) films from triphenylamine based electroactive compounds for electrochromic applications. Polymers, 2017, 9(12), pp. 708. DOI: https://doi.org/10.3390/polym9120708
50. Patrick S.; Curley M. Exotic ground states and excitations in quantum magnets. Thesis for the degree of Doctor of Philosophy, the University of Warwick, Department of Physics, England, 2021, pp. 139. http://wrap.warwick.ac.uk/164319
51. Hirata H.; Kuyama T.; Ono M.; Shimoyama Y. Detection of electron paramagnetic resonance absorption using frequency modulation. Journal of Magnetic Resonance, 2003, 164(2), pp. 233–241. DOI: 10.1016/s1090-7807(03)00236-2